Acta Crystallographica Section B
Structural Science
ISSN 0108-7681

Structures of the cubic and rhombohedral high-pressure modifications of silicon as packing of the rod-like substructures determined by the algebraic geometry

V. S. Kraposhin,[a]* A. L. Talis,[b] V. G. Kosushkin,[a] A. A. Ogneva[a] and L. I. Zinober[c]

[a]Bauman Moscow State Technical University, 5 Second Baumanskaya St., Moscow 105005, Russia, [b]A. N. Nesmeyanov Institute of Organoelement Compounds, Russian Academy of Sciences, Moscow, Russia, and [c]All-Russian Research Institute for Synthesis of Minerals, Alexandrov, Vladimir District, Russia

Correspondence e-mail: kraposhin@mtu-net.ru

Received 30 July 2007
Accepted 16 November 2007

Tessellations by generating clusters are proposed for the high-pressure phases BC8 and R8 of silicon. The structures of both high-pressure phases are represented by the parallel packings of rods. The latter are stacks of distorted icosahedra, joined by a common triangular face and flattened out along the threefold symmetry axis. Along the rod axis there is an alternation of empty and double-centered icosahedra. The empty icosahedra are additionally distorted in the cubic BC8 phase by antiparallel rotation about the rod axis, while the double-centered icosahedra are distorted by that rotation in the rhombohedral R8 phase. A possible mechanism of the reversible BC8 $\leftrightarrow$ R8 transformation is proposed as the rotation about the rod axis of the common triangular face of the neighboring icosahedra, thus transforming between distorted and undistorted icosahedra. The graphs of the generating clusters for both the BC8 and R8 structures are determined by two subconfigurations of the same construction of the finite projective geometry.

1. Introduction

Silicon with the cubic diamond structure (Si-I) transforms into the β-Sn modification Si-II at high pressure. During depressurization the reverse transformation into the cubic diamond structure does not occur. Instead, the transformation sequence Si-II $\rightarrow$ R8(Si-XII) $\rightarrow$ BC8(Si-III) was observed. The metastable phases R8 and BC8 have rhombohedral (space group $R3$) and body-centered cubic (space group $Ia3$) structures, respectively. A complete description of the high-pressure phase diagrams of carbon, silicon and germanium can be found in the review paper by Mujica *et al.* (2003). The BC8 phase of silicon can exist under ambient pressure conditions, so heating must be applied for the recovery of the stable cubic diamond modification.

The difference in the sequence of the phase transformations between the pressure application and pressure release is due to the mechanisms of the phase transformations and the features of the structures of the high-pressure phases. The structure of the cubic BC8 phase can be described as composed of 14-vertex clusters, which are a combination of an octahedron and a hexagonal bipyramid (see Fig. 1). The sixfold axis of the bipyramid is parallel to one of four threefold axes of the BC8 crystal structure (Kasper & Richards, 1964; Crain *et al.*, 1994). The structure of the rhombohedral R8 phase can be described as composed of 14-vertex clusters with an inner edge. The inner edge forms by the movement of two atoms in opposing directions along the threefold axis (the opposite sixfold vertices of the hexagonal bipyramid in Fig. 1) into the interior of a cluster. This opposing movement along the threefold axis was regarded as the mechanism of the BC

↔ R8 phase transformation by Crain *et al.* (1994) and Dmitrienko & Kléman (1999). This transformation between two metastable phases is reversible with pressure.

Actually, this scenario of the BC ↔ R8 phase transformation through one-dimensional atomic movements cannot describe all the features of this transformation. There are four non-intersecting threefold symmetry axes in the space group *Ia*3 of the BC8 phase, hence the atomic jumps along four different threefold axes have equal probabilities. These atomic jumps along different threefold axes must be correlated in space to form a finite volume of the new R8 phase. However, the mechanism based on one-dimensional atomic movement does not take into account this correlation.

Moreover, even if the atoms move along only one of the four threefold axis this mechanism does not describe the reconstruction of the whole three-dimensional structure during the BC ↔ R8 phase transformation. Each one of the two moving vertices of the hexagonal bipyramid in Fig. 1 is shared by three hexacycles of a given cluster. The tessellation of the BC8 crystal space into 14-vertex clusters supposes the joining of clusters along common hexacycles in such a way that a sixfold vertex of the bipyramid (of a given cluster) is shared by four 14-vertex clusters. Thus, opposite atomic displacements along one threefold axis gives rise to not only atomic penetration inside the empty 14-vertex cluster, but it also changes the structure of the other clusters sharing the hexacycles with the given cluster. The displaced atoms also belong to the basement of the hexagonal bipyramid and *vice versa*, the parallel displacement of the sixfold vertices of the 14-vertex clusters neighboring the given cluster is a displacement of the basement vertices of the given cluster at the same time. In other words, the model proposed by Crain *et al.* (1994) and Dmitrienko & Kléman (1999) does not describe all the symmetry features of the BC ↔ R8 phase transformation.

Figure 1
Generating cluster for the crystalline structure BC8 with 14 vertices as an octahedron and a hexagonal bipyramid join with a common triad axis. Light vertices with the numbers 1, 2, 7, 4, 5 and 6 belong to the octahedron, black vertices with the numbers 1, 5, 3, 2, 6, 8, 4 and 7 belong to the hexagonal bipyramid. Vertices 4 and 7 are situated on the triad axis. The derivation of the cluster from the constructions of projective geometry is described in the *Appendix*.

Space-group symmetry is not able to describe all these symmetry features, because in general various tessellations into various polyhedra would correspond to the same orbit of the space group. The fundamental insufficiency of space-group symmetry in providing a complete description of the crystal structure tessellation was demonstrated by Delgado Friedrichs *et al.* (1999) with the utilization of constructions of the algebraic geometry. The existence of other tessellations of the BC8 structure besides the above-described tessellation onto the 14-vertex clusters, and the fact that other tessellations could describe all the indicated symmetry features of the BC↔R8 phase transformation, has been suggested. The present paper reports a new structure model which completely describes the symmetry features of this transformation. The model is based on alternative tessellations for the BC8 and R8 phases that were obtained by the methods of algebraic (finite projective) geometry. A similar approach has been used for the description of polymorphic transformations in iron (Kraposhin *et al.*, 2002) and titanium (Kraposhin *et al.*, 2006), and for the description of the metal melting (Kraposhin *et al.*, 2007).

2. A generating cluster and the tessellation of the BC8 structure into rods

The determination of a tessellation requires the determination of generating polyhedra for this tessellation. A 14-vertex cluster has been described, *i.e.* the numbers of vertices, edges and faces have been given, but this does not uniquely define the cluster as the numbers of vertices, edges and faces can be equal for two polyhedra, with a different number of edges meeting at one vertex.

To define a polyhedron means to define its graph, *i.e.* the set of vertices and edges connecting these vertices. In the framework of a space group theory the 14-vertex cluster of the BC8 structure cannot be determined, since 7 is not an order of the point crystallographic group. However, it is known that the cubic diamond structure with the space group *Fd*3*m* can be tessellated onto 14-vertex non-convex parallelohedra (O'Keeffe, 1999). This 14-vertex cluster is derived from the construction of projective geometry in the *Appendix*. It is not the unit cell, but it generates the cubic diamond structure by parallel translations along three directions in space. Thus, it is a translationally equivalent fragment of the diamond structure, although the point subgroups of the *Fd*3*m* space group do not determine this 14-vertex cluster.

This example shows that the unit cell does not give a full description of the given structure. A complete symmetry description of the structure is determined not by the orbits of the space group, but by the joining of polyhedra. This joining of polyhedra is determined uniquely by the single construction of the algebraic geometry. Graphs of some polyhedra are most conveniently represented within the language of the theory of configuration. A summary of the concepts and notations of the theory of configurations is given in the *Appendix* (see also Kárteszi, 1976).

It was shown recently by Talis (2002*a*,*b*) that 14-vertex clusters of the cubic diamond structure and the BC8 structure are the Euclidian realisations of the constructions of finite projective geometry. A procedure for the derivation of generating clusters for diamond-like structures from the constructions of projective geometry is also given in the *Appendix*.

Delineation of this 14-vertex cluster in the unit cell of the BC8 structure is shown in Fig. 2. The cubic BC8 structure has four threefold axes, however, the 14-vertex cluster has only one threefold symmetry axis and also this cluster is not a parallelohedron, *i.e.* it cannot serve as a translationally equivalent part of the BC8 structure. The BC8 structure can then be tessellated onto rods containing 14-vertex clusters. The symmetry group of each rod is $p32$, where p is the one-dimensional group of translations along $\langle 111 \rangle$. Since the 14-vertex clusters belonging to one rod are isolated from each other, another cluster is generated between two neighboring 14-vertex clusters and one obtains a rod consisting of alternating clusters of two types (Fig. 3). One type of cluster is the 14-vertex cluster (lighter shading in Fig. 3). Two vertices of this cluster belonging to the threefold axis of the cubic structure penetrate into the interior of two neighboring clusters of the other type (the dark cluster in Fig. 3). So, this cluster contains an inner edge connecting two vertices situated on the threefold axis, which also has 14 vertices. Two neighboring clusters of different types have a common triangular face which is normal to $\langle 111 \rangle$ (the triangular face of the octahedron in Fig. 1).

These rods formed by two different clusters are not isolated from each other. Actually they have common vertices with similar parallel rods, and parallel packing of these rods describes the BC8 crystal structure (Fig. 4). The rod of clusters now serves as the translationally equivalent part of the structure.

3. Icosahedral clusters in the BC8 structure

Delineation of the bicapped icosahedron in the empty 14-vertex cluster can also be described within the theory of configurations (see the *Appendix*). The icosahedron is distorted by compression along its threefold symmetry axis and by rotation of six vertices on 36.650 about the $\langle 111 \rangle$ direction. As a result of this deformation the icosahedral symmetry is lowered towards $\bar{3}$. The double-centered icosahedron (the icosahedron having an inner edge, see Fig. 5*b*) has the higher symmetry $\bar{3}m$.

The centered icosahedron is rotated relative to the empty icosahedron by 60° since they share a common face. Congruent tetrahedral holes arise between the rods. The centers of that tetrahedra belong to a single orbit of the space group $Ia3$. Thus, the BC8 structure determines the tessellation of the three-dimensional Euclidian space onto two types of icosahedra and one tetrahedron. It can be easily seen that the crystal structures of both BC8 and R8 can be represented by topologically equivalent tesselations. Indeed, when the reverse rotation of the triangular faces {111} of the empty icosahedra about their normal occurs, thus restoring their mirror planes, the respective rotation occurs simultaneously in double-centered icosahedra of the same rod, thus eliminating mirror planes in these icosahedra. This rotation which occurs in all icosahedra of a given rod converts the BC8 structure into the structure of the rhombohedral R8 phase, which is the representation of the same joining of rods formed by empty and double-centered icosahedra. After rotation the R8 structure is obtained, in which the empty icosahedron in the R8 phase

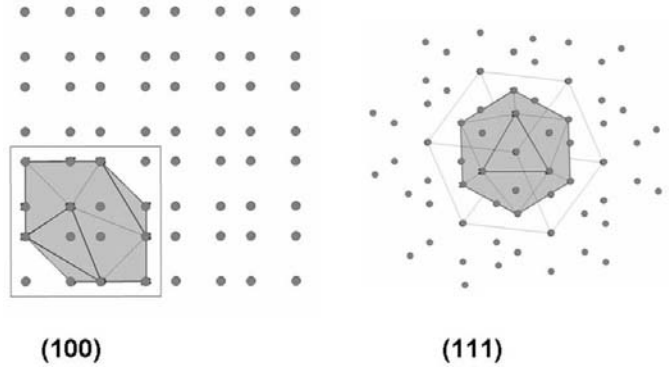

Figure 2
Projections of the cubic BC8 structure along twofold and threefold symmetry axes. A delineation of the unit cell and 14-vertex cluster is shown.

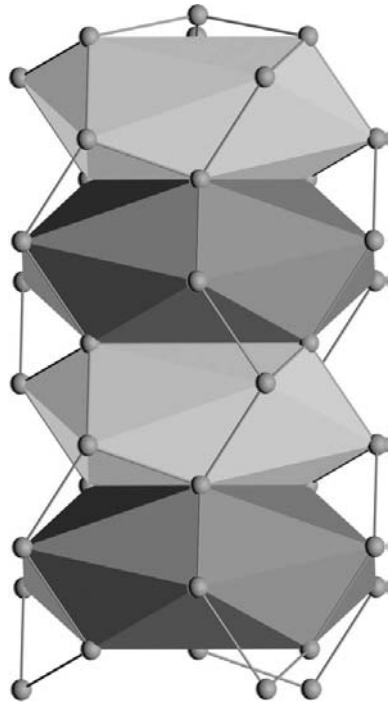

Figure 3
The translationally equivalent rod in the BC8 structure is the alternate stacking of empty (light) and double-centered (dark) 14-vertex clusters along the $\langle 111 \rangle$ direction. Note the tetrahedral cap on the empty light cluster. The second cap of the same cluster is on the opposite triangular {111} face, *i.e.* it penetrates into the interior of the neighboring dark cluster.

shows $\bar{3}m$ symmetry while the centered icosahedron actually has $\bar{3}$ symmetry. In other words, with the absence of centered atoms inside icosahedra, structures of BC8 and R8 phases are not distinguishable (not taking into account atomic relaxations). The mathematical foundation for the similarity of these two structures is based on the fact that the crystal structures of BC8 and R8 phases can be generated by repeating the clusters having identical graphs which are determined by two subconfigurations of the same finite projective geometry.

The approximate Miller indices for the faces of both 14-vertex clusters are shown in Fig. 5. Twelve faces of the empty two-capped icosahedron have indices of the types {853} and {532}, *i.e.* in correspondence with the Fibonacci series (Fig. 5*a*). The same indices describe 24 out of the 30 faces of a triacontahedron in a cubic setting, *i.e.* when the remaining six faces are {100}. Six faces of the icosahedron also have {100} indices. Miller indices of the inclined faces of the tetrahedral cap (not shown) are {964}.

The present model for the BC8–R8 transformation involves the rotation of a common triangular face of two neighboring icosahedra of a single rod. It implies the displacement of atoms belonging to neighboring rods, *i.e.* it defines the structural deformations governing the phase transition.

According to Dmitrienko & Kléman (1999), the rhombohedral R8 structure has one feature, namely the presence of five-membered atomic rings. Five-membered rings in the BC8 and R8 phases are shown in Figs. 6 and 7. The five-membered ring of the shortest interatomic bonds in the R8 phase includes the inner edge of a 14-vertex cluster. The respective five-membered atomic complex of the BC8 phase includes an edge with a length approximately 1.5 times larger than the other four edges. Rotation of the triangular face about the threefold symmetry axis ensures an equalization of bond lengths in this complex, thus converting the BC8 phase into the R8 phase.

The proposed tesselation of both structures into rods is in accordance with the concept of O'Keeffe & Andersson (1977) which considers a crystal as the stacking of congruent infinite cylinders (rods). The linear transport theorem can be regarded as the mathematical foundation for this rod concept. In accordance with this theorem only linear (rod-like) substructures of n-dimensional constructions ($n > 3$) can be mapped onto the three-dimensional Euclidian space E^3 with minimal distortions (Kléman, 1989). In the {3, 3, 5} polytope (a four-dimensional counterpart of an icosahedron) each vertex is the center of a regular icosahedron. As a result, the {3, 3, 5} polytope contains the icosahedra joined in a face-to-face mode along the common symmetry axis 6_1. While mapping onto E^3,

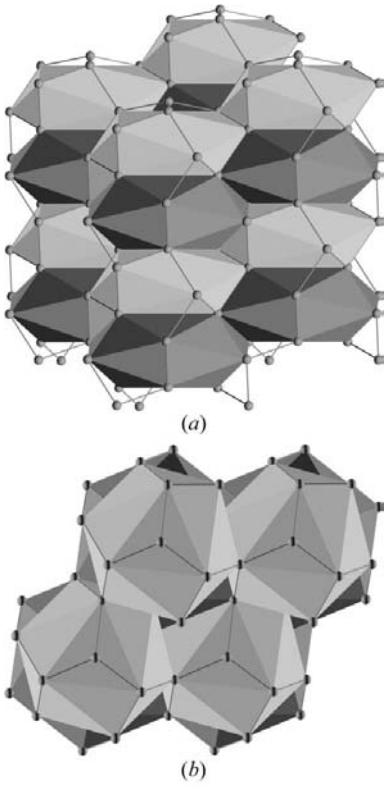

Figure 4
Parallel dense packing of translationally equivalent rods generates the crystal structure of the BC8 phase: views along (*a*) the normal and (*b*) parallel to the [111] axis.

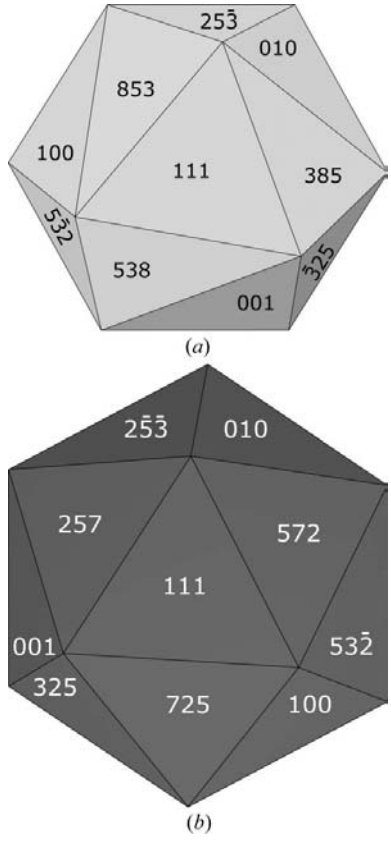

Figure 5
(*a*) The condition for the equality of edge lengths is violated in the BC8 crystal structure, hence the 14-vertex cluster can be represented as the empty icosahedron flattened out along ⟨111⟩ with two tetrahedral caps on the opposite parallel {111} faces (not shown here, see Fig. 3). The symmetry of the icosahedron is $\bar{3}$. Approximate Miller indices are inscribed on the respective faces. (*b*) An icosahedron with the inner edge and $\bar{3}m$ symmetry. Approximate Miller indices are shown on the respective faces. The icosahedron is centered by the vertices of tetrahedral caps from two neighboring empty icosahedra, as shown in (*a*). Two centering atoms form the inner edge. The empty and centered icosahedra share the common {111} face.

this icosahedral joining from {3, 3, 5} determines a rod formed by centered icosahedra with the common threefold axis. The rod in the BC8 structure will be congruent with the rod from {3, 3, 5} when all icosahedra in the BC8 structure become regular and single centered.

4. Conclusion

(i) Tessellations onto generating clusters have been derived for the high-pressure BC8 and R8 phases of silicon. The structures of both high-pressure phases were represented as parallel packings of rods that are made of icosahedra with common triangular faces. The icosahedra are flattened out along the threefold symmetry axis which is normal to the common triangular face. There is an alternation of empty and double-centered icosahedra along the rod axis, and each second icosahedron is distorted by antiparallel rotation about the rod axis.

(ii) The empty icosahedra are twisted in the structure of the cubic BC8 phase, and the double-centered icosahedra are twisted in the structure of the rhombohedral R8 phase. A possible mechanism of the reversible BC8 $\leftrightarrow$ R8 transformation is proposed as the rotation of the common triangular face of the neighboring icosahedra. The rotation of the common triangular face destroys the mirror plane in one icosahedron and restores the mirror plane in the other.

(iii) Graphs of the generating clusters for both BC8 and R8 structures are determined by the same construction of the finite projective geometry. The experimentally observed reversibility of mutual transformations between high-pressure phases BC8 and R8 can be determined by the relationship between generating clusters.

APPENDIX *A*

A structure containing n points $P_1, P_2, \ldots, P_n$ and n straight lines $l_1, l_2, \ldots l_n$, in which $q + 1$ straight lines consist of $q + 1$ points running through each point, is said to be a finite projective plane $PG(2,q)$ of the order q. The line l_i can be broken (polygonal), and the relation $n = q^2 + q + 1$ is fulfilled between n and q. The projective plane $PG(2,q)$ is defined uniquely by its incidence table which is a square table $n \times n$ with columns $P_1, P_2, \ldots, P_n$ named as points and rows $l_1, l_2, \ldots l_n$ as straight lines. The incidence of point P_i and straight line l_j is designated by filling a cell ij of this table (by an incidence sign); an empty cell signifies the absence of incidence. A configuration can be used as a graphic model of the finite projective plane which is a set of m points and n straight lines (planes), in which c straight lines (planes) run through each point, while d points belong to each straight line (plane). The configuration is designated as (m_c, n_d). If $m = n$ the configuration is self-dual and designated as $\{n_d\}$. The configuration is defined by its incidence table $\Gamma(m_c, n_d)$ consisting of m rows and n columns, and containing $mc = nd$ incidence signs. The configuration can be realised in different spaces (both finite and infinite). The configuration must be geometrical so that it can be realised on any projective plane. The geometrical configuration means that its incidence table $\Gamma(m_c, n_d)$ contains an empty cell in its sub-table 2×2. This condition ensures the intersection of two different straight lines of the projective plane at only one point.

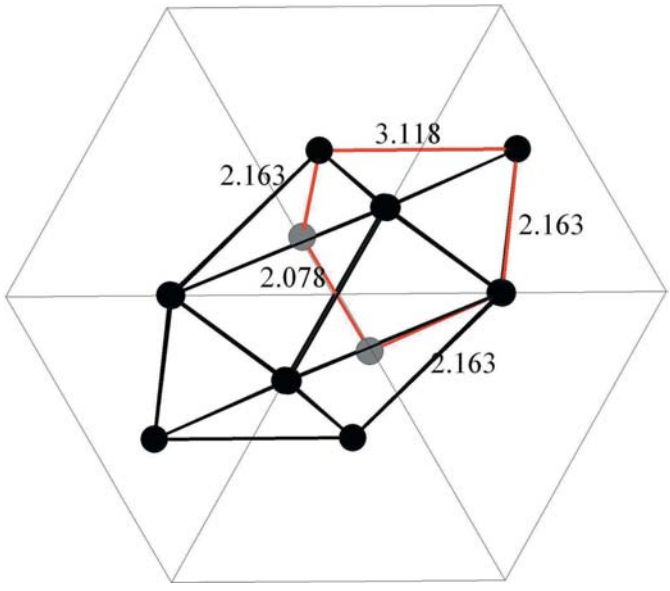

Figure 6
Delineation of the fivefold cycle in the cubic BC8 structure (shown in red). Numbers show the edge length in Å. It can be seen that one edge is 1.5 times longer compared with the other edges, *i.e.* this edge is not the shortest bond in the BC8 structure.

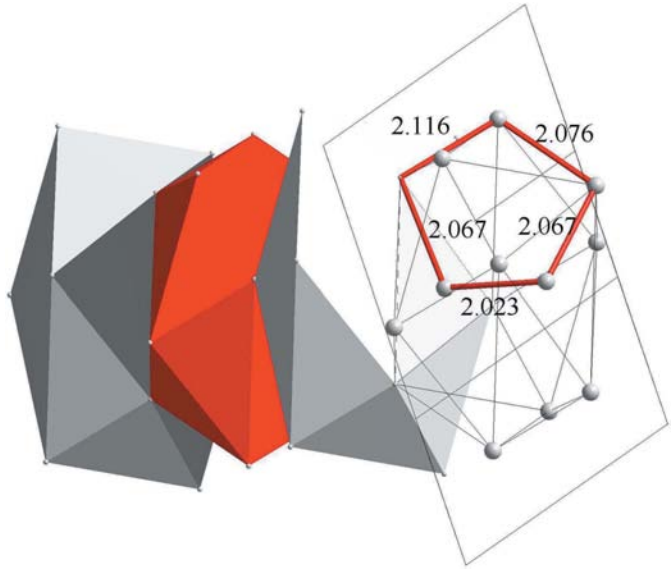

Figure 7
Delineation of the fivefold cycle in the rhombohedral R8 structure (shown in red). Numbers show the edge length in Å. The alternating empty and double-centered icosahedra along the triad axis are also shown. The icosahedron with the inner edge is shown in red.

As an example, the finite projective plane $PG(2,2)$ or the self-dual Fano configuration $\{7_3\}$ is shown in Fig. 8 together with its incidence table. Parallel straight lines l_2 and l_5, l_3 and l_6, and l_7 and l_4, respectively, intersect at ideal points 0, 1, ∞, which form an infinitely distant straight line l_1 (a dotted line). In projective geometry an infinite Euclidian plane is complemented with an infinitely distant straight line, and parallel straight lines belonging to that Euclidian plane intersect on this distant straight line. For projective geometry the duality principle holds: if the words 'point' and 'straight line' are interchanged everywhere, all definitions and theorems will remain unchanged. This principle permits using the incidence table of $PG(2,q)$ to construct a graph as a model for this $PG(2,q)$. For that, points P_1, $P_2 \ldots$, P_n, and straight lines l_1, $l_2 \ldots$, l_n, of $PG(2,q)$ are taken to be the white and black vertices of the graph, and those and only those pairs from one light and one black vertex will be connected by the graph edge, for which there is an incidence sign at the intersection of the respective row l_i and column P_j. Skipping of the graph edge or substituting the filled incidence sign by the unfilled incidence sign means an extermination of the respective segments of the straight line. The incidence table in Fig. 8(*b*) contains three unfilled circles substituting incidence signs. It means the extermination segments of straight lines l_2, l_3, l_4 in between

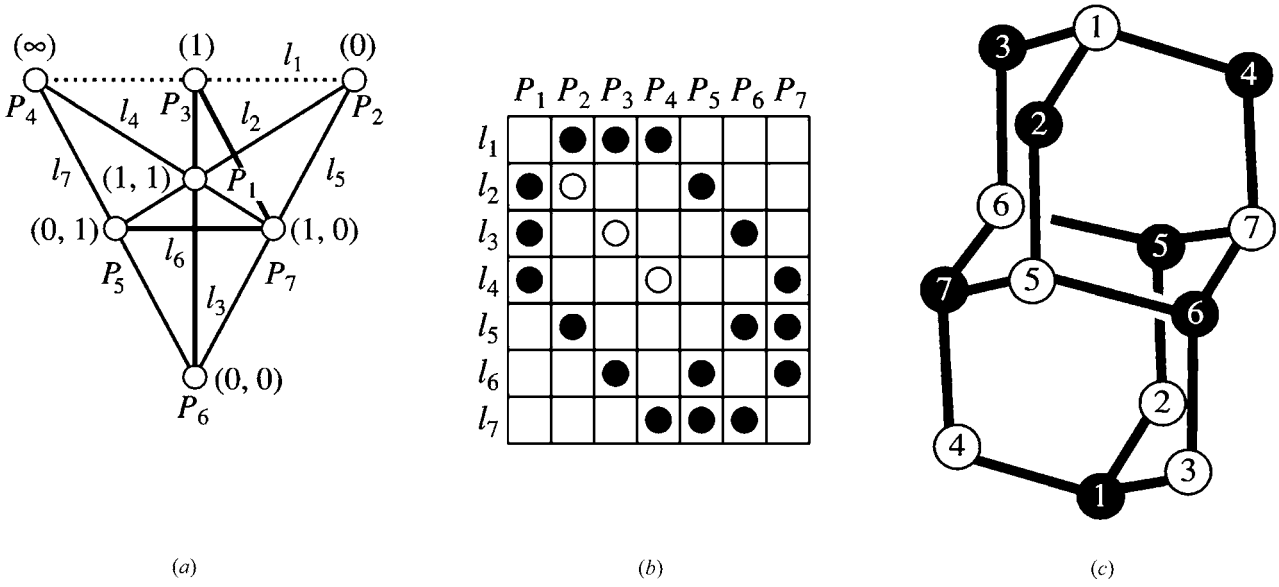

Figure 8
(*a*) Graphic model of the finite projective plane $PG(2,2)$ or autodual Fano configuration $\{7_3\}$. Parallel straight lines l_2, l_5; l_3, l_6; l_7, l_4 intersect at ideal points 0, 1, ∞, forming an infinitely distant straight line. (*b*) The incidence table for $PG(2,2)$. A removal of three incidence signs (empty circles) means the annihilation of the line segments l_2, l_3, l_4 in between P_1 and P_2, P_3, P_4. The parallel straight lines l_2 and l_5, l_4 and l_7, l_3 and l_6 do not intersect at ideal (infinitely distant) points P_2, P_4, P_3. (*c*) Graph of the 14-vertices cluster of the diamond structure as the realisation of the configuration mapped by the incidence table (*b*).

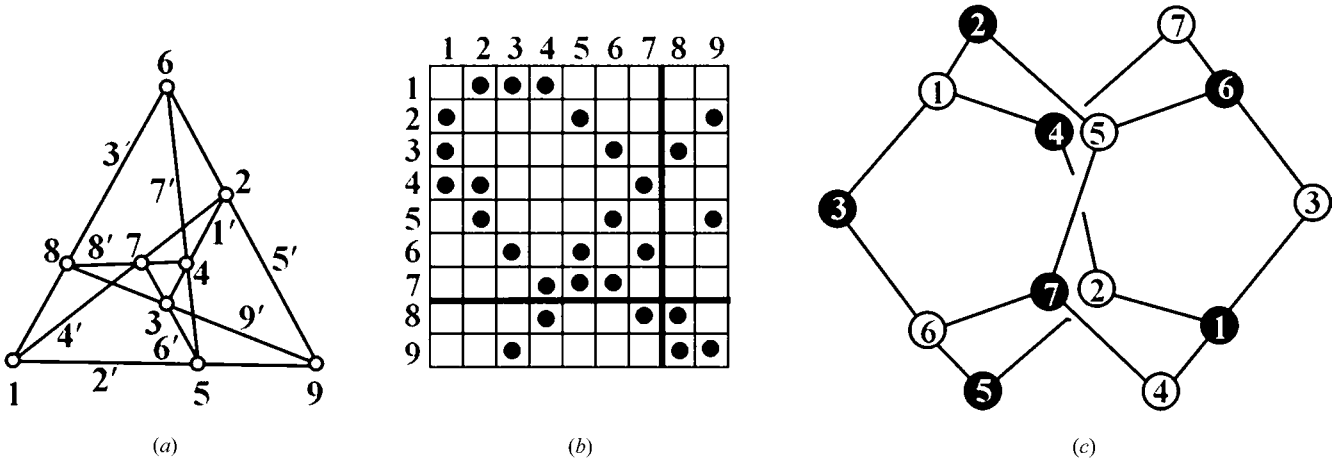

Figure 9
(*a*) An irregular $\{9_3\}_3$ configuration and (*b*) its incidence table. The sub-table 7×7 (shown by thick lines) defines a 'faulted' diamond cluster, which coincides with the core of a screw dislocation in the diamond structure. Primed numbers in (*a*) designate straight lines corresponding to the black vertices of the cluster.

points P_1 and P_2, P_3, P_4. Then parallel straight lines l_2 and l_5, l_4 and l_7, and l_3 and l_6 will not intersect in ideal (infinitely distant) points P_2, P_4, P_3. In other words, the extermination of three incidence signs corresponds to passing from projective to Euclidian geometry (Euclidian mapping of the projective plane $PG(2,q)$.

The construction of the bichromatic graph from white and black points by using the incidence table generates a cluster with 14 vertices (Fig. 8*c*). This cluster is the non-convex parallelohedron representing the joining of seven non-convex hexacycles in the chair conformation. While translated by the f.c.c. lattice this 14-vertex cluster generates a diamond structure.

In a similar way, the generating cluster of the BC8 structure can be derived from a so-called irregular self-dual configuration $\{9_3\}_3$ (Fig. 9*a*). The sub-table 7×7 can be delineated in the incidence table of this configuration (Fig. 9*b*). The graph of this sub-table (Fig. 9*c*) determines a 'faulted' 14-vertex diamond cluster. When translating this cluster along the $\langle 110 \rangle$ direction of the diamond structure, a linear substructure is generated coinciding exactly with the core of a screw dislocation in the diamond structure (Hornstra, 1958). In such a sense the 'faulted' cluster shown in Fig. 9(*c*) can be regarded as the generating cluster of the screw dislocation in the diamond structure. Displacement of column 3 beyond column 9 gives the isomorphic incidence table (Fig. 10*a*).

Now, a sub-table 8×6 is delineated in this transformed isomorphic table. This 8×6 incidence table defines a non-self-dual configuration which can be considered as an intersection between the $\{9_3\}_3$ configuration and the $(6_4,8_3)$ configuration. The incidence table of the $(6_4,8_3)$ configuration is shown in Fig. 10(*b*). Unfilled circles in this table designate the incidence signs which are absent in the incidence table of Fig. 10(*a*). The configuration $(6_4,8_3)$ defines (by both unfilled and filled incidence signs) the graph of a rhombic dodecahedron, *i.e.* in this cluster there are two kinds of vertices: six vertices have four edges meeting at them, and eight vertices have three edges meeting at them.

On skipping six edges of the rhombic dodecahedron (unfilled circles in the table correspond to skipped edges) a graph i was obtained representing the joining of two graphs: a hexagonal bipyramid and an octahedron, both having the common triad axis (Fig. 10*c*). By superimposing the condition of the maximal possible equality of edge lengths and angles between them, the graph obtained determines the generating cluster of the BC8 structure.

It can easily be shown that a delineation of the two-capped icosahedron in the 14-vertex generating cluster of the BC8 structure is determined by the incidence table for the subconfiguration from the $(6_4,8_3)$ configuration, which in turn determines the whole cluster. Indeed, three incidence signs are situated only in the fourth and seventh rows of this table, therefore they single out two vertices positioned on the triad axis. The remaining 12 vertices are the vertices of the icosahedron, and between the edges of this icosahedron there are six edges of the rhombic dodecahedron which are omitted in Fig. 10.

The work has been carried out with the financial support of the Russian Foundation for Basic Research (RFBR grants 05-03-32539 and 05-02-17141), program 7 of the Division of Chemical Sciences of Russian Academy of Science and 'The innovation support-2007' program of the Russian Academy of Science

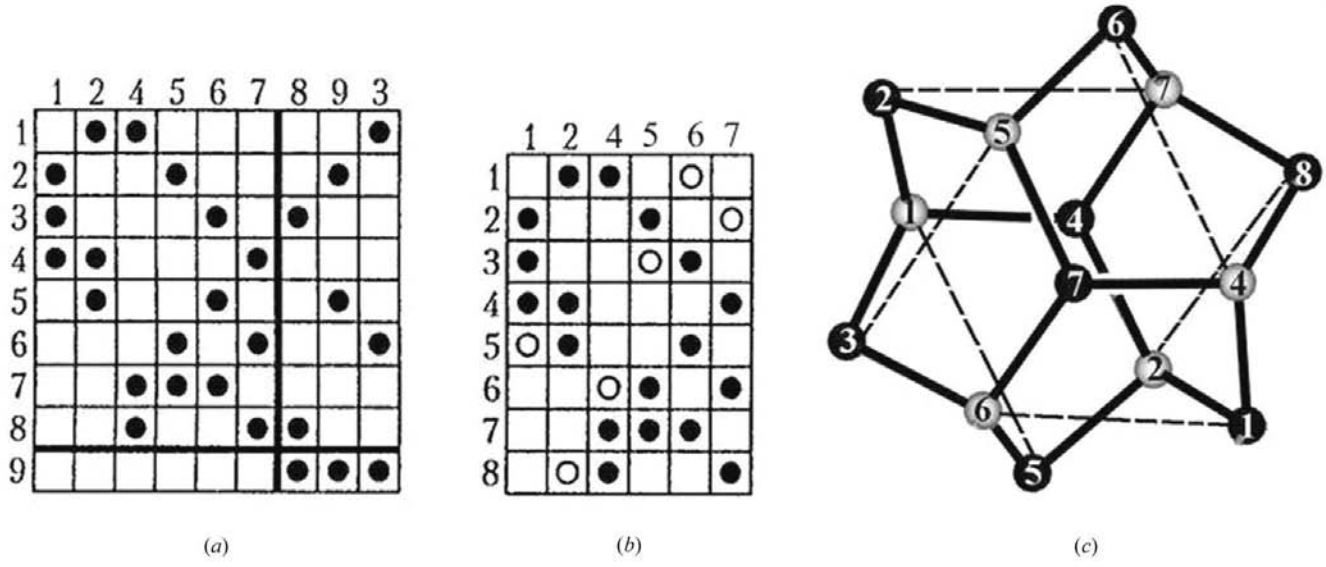

Figure 10
(*a*) Transformation of the incidence table of the $\{9_3\}_3$ configuration results in the generating cluster of the BC8 structure. The third column is displaced beyond the ninth column, so the isomorphic incidence table is formed. The sub-table 6×8 is delineated by thick lines; this 6×8 sub-table determines the generating cluster of the BC8 structure. (*b*) The incidence table of the non-geometrical $(6_4, 8_3)$ configuration determines the graph of a rhombic dodecahedron. After skipping six edges (unfilled circles), this table coincides with the sub-table 6×8 in (*a*); (*c*) The generating cluster of the BC8 structure is determined by the intersection of incidence tables for $\{9_3\}_3$ (*a*) and $(6_4, 8_3)$ (*b*) configurations. Dotted lines are the edges of the incidence graph for the $(6_4, 8_3)$ configuration (edges of the rhombic dodecahedron) which correspond to the unfilled circles in the incidence table in (*b*).

References

Crain, J., Ackland, G. J., Maclean, J. R., Piltz, R. O., Hatton, P. D. & Pawley, G. S. (1994). *Phys. Rev. B*, **50**, 13043–13046.

Delgado Friedrichs, O., Dress, A. W. M., Huson, D. H., Klinowski, J. & Mackay, A. L. (1999). *Nature*, **400**, 644–647.

Dmitrienko, V. E. & Kléman, M. (1999). *Philos. Mag. Lett.* **79**, 359–367.

Hornstra, J. (1958). *J. Phys. Chem. Solids*, **5**, 129–141.

Kárteszi, F. (1976). *Introduction to Finite Geometries*. Budapest: Akadémiai Kiadó.

Kasper, J. S. & Richards, S. M. (1964). *Acta Cryst.* **17**, 752–755.

Kléman, M. (1989). *Adv. Phys.* **38**, 605–667.

Kraposhin, V. S., Talis, A. L. & Dubois, J.-M. (2002). *J. Phys. Condens. Matter*, **14**, 8987–8996.

Kraposhin, V. S., Talis, A. L. & Samoylovitch, M. I. (2007). *J. Non-Cryst. Solids*, **353**, 3279–3284.

Kraposhin, V. S., Talis, A. L. & Wang, Y. J. (2006). *Mater. Sci. Eng. A*, **438–440**, 85–89.

Mujica, A., Rubio, A., Muñoz, A. & Needs, R. J. (2003). *Rev. Mod. Phys.* **75**, 864–912.

O'Keeffe, M. (1999). *Z. Kristallogr.* **214**, 438–442.

O'Keeffe, M. & Andersson, S. (1977). *Acta Cryst.* A**33**, 914–923.

Talis, A. L. (2002*a*). *Cryst. Rep.* **47**, 527–536.

Talis, A. L. (2002*b*). *Cryst. Rep.* **47**, 775–784.